Supplementary Information

Qualitative Trends versus Quantitative Accuracy: A Case Study of $LiMn_{1.5}Ni_{0.5}O_4$ Cathode Material

Adama GASSAMA[1], Etienne MANGAUD[1], Alexander MITRUSHCHENKOV[1], Céline LEONARD[1], Emmanuelle SUARD[3], Régis POULAIN[2], Stéphane BACH[2,4], and Nicolas EMERY[1,2,*]

[1]Univ Gustave Eiffel, Univ Paris Est Creteil, CNRS, UMR 8208, MSME, F-77454 Marne-la-Vallée, France
[2]Univ Paris Est Creteil, CNRS, ICMPE (UMR 7182), 2 rue Henri Dunant, F-94320 Thiais, France
[3]Institut Laue-Langevin, BP 156, 38042 Grenoble, France
[4]Université Paris Saclay - Evry, Dept Chimie, Bd F. Mitterrand, 91000, Evry, France
[*]Corresponding author: nicolas.emery@cnrs.fr

March 16, 2026

1 Crystal structure within the $P4_332$

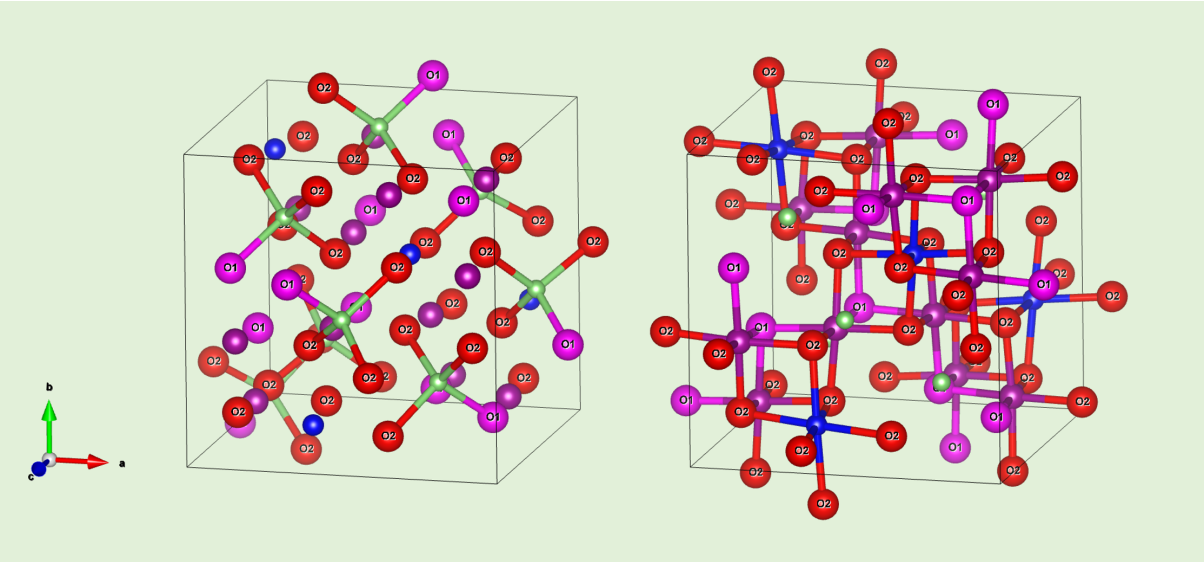

Figure SI.1: representations of the crystal structure of $LiMn_{1.5}Ni_{0.5}O_4$ within the $P4_332$ space group. Green spheres are lithium, purple spheres are manganese, blue spheres are nickel, pink sphere are oxygen O1 and red spheres are oxygen O2. Left side, only the Li-O bonds are plotted. Right side, Ni-O and Mn-O are displayed.

2 Energies of the possible lithium distributions in $Li_{0.5}Mn_{1.5}Ni_{0.5}O_4$

Various lithium distributions were calculated according to the work of Kishida *et al.* [1]. Calculations were performed using PBE functional and the lithium distributions are labelled according Kishida *et al.*. As indicated by Table SI.1, the configuration which exhibits the lowest energy is obtained with a homogeneous distribution of the lithium into the available tetrahedral sites: half of the sites are filled without two successive sites being filled.

Config.	Lithium positions	Energy E (eV/unit cell) ΔE (E-E_{min}, *eV/unit cell*)
4I	(0 0 0) (1/2 1/2 0) (1/4 1/4 1/4) (3/4 3/4 1/4)	-378.84067 *0.2939*
4J	(0 0 0) (1/2 1/2 0) (1/4 1/4 1/4) (1/2 0 1/2)	-378.83197 *0.3026*
4K	(0 0 0) (1/2 1/2 0) (1/4 1/4 1/4) (3/4 1/4 3/4)	-378.7089 *0.4256*
4L	(0 0 0) (1/2 1/2 0) (1/4 1/4 1/4) (1/4 3/4 3/4)	-378.8247 *0.3098*
4M	(0 0 0) (1/2 1/2 0) (3/4 3/4 1/4) (1/2 0 1/2)	-378.9656 *0.1689*
4N	(0 0 0) (1/2 1/2 0) (3/4 3/4 1/4) (1/4 3/4 3/4)	-378.9579 *0.1766*
4O	(0 0 0) (1/2 1/2 0) (1/2 0 1/2) (0 1/2 1/2)	-379.1345 *0*

Table SI.1: calculated energies E of $Li_{0.5}Mn_{1.5}Ni_{0.5}O_4$ and energy difference ΔE between the lowest energy configuration E_{min} and the considered energy E for different lithium distributions in the cell (PBE functional). A homogeneous distribution (4O configuration) leads to the lowest energy.

3 Energies of the magnetic configurations for the three Li compositions

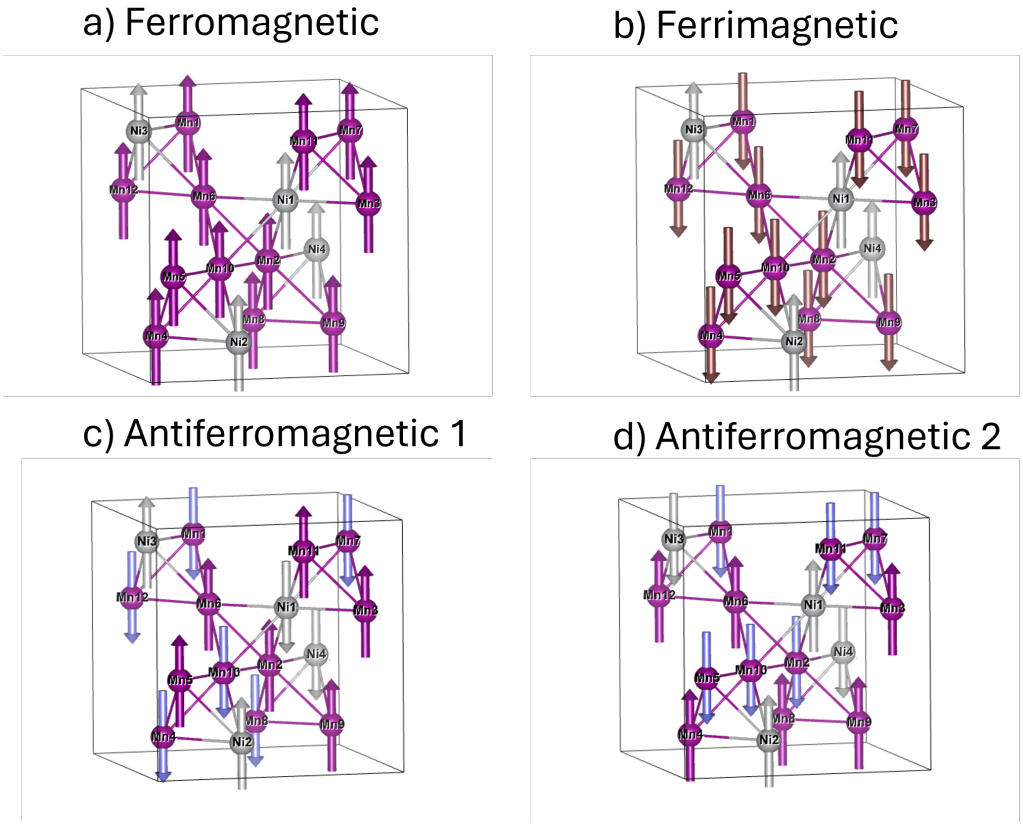

Figure SI.2: different magnetic configurations used for ground state calculations. (a) Ferromagnetic, (b) Ferrimagnetic, (c) Antiferromagnetic 1 (AFM1) and (d) Antiferromagnetic 2 (AFM2). Vector length are not related to the magnetic moment values and are here just for illustration.

	$LiMn_{1.5}Ni_{0.5}O_4$	$Li_{0.5}Mn_{1.5}Ni_{0.5}O_4$	$Mn_{1.5}Ni_{0.5}O_4$
FM	-401.2144	converges in FiM	-355.1612
FiM	**-402.2838**	-378.9696	–
AFM1	-401.2362	**-379.1345**	-355.3216
AFM2	-401.7632	-379.0988	**-355.5292**

Table SI.2: Energy calculated using PBE functional with various initial magnetic structure (eV). Bold values are the minimum value for each composition. FM: ferromagnetic, FiM: ferrimagnetic, AFM1: antiferromagnetic 1, AFM2: antiferromagnetic 2.

	$LiMn_{1.5}Ni_{0.5}O_4$	$Li_{0.5}Mn_{1.5}Ni_{0.5}O_4$	$Mn_{1.5}Ni_{0.5}O_4$
FM	-361.6723	**-334.7370**	**-308.2285**
FiM	**-361.9626**	-334.5949	–
AFM1	-361.5915	-334.6600	-307.8569
AFM2	-361.4829	-334.5398	-307.9198

Table SI.3: Energy calculated using PBE+U functional with various initial magnetic structure (eV). Hubbard parameters were U_{Mn} = 3.9 eV and U_{Ni} = 6.2 eV. Bold values are the minimum value for each composition. FM: ferromagnetic, FiM: ferrimagnetic, AFM1: antiferromagnetic 1, AFM2: antiferromagnetic 2.

	$LiMn_{1.5}Ni_{0.5}O_4$	$Li_{0.5}Mn_{1.5}Ni_{0.5}O_4$	$Mn_{1.5}Ni_{0.5}O_4$
FM	-551.0360	-523.2703	-495.8771
FiM	**-551.6037**	-523.6335	–
AFM1	-551.2838	**-523.6989**	-495.8496
AFM2	-551.2542	-523.6168	**-496.0066**

Table SI.4: Energy calculated using r^{2}SCAN functional with various initial magnetic structure (eV). Bold values are the minimum value for each composition. FM: ferromagnetic, FiM: ferrimagnetic, AFM1: antiferromagnetic 1, AFM2: antiferromagnetic 2.

	$LiMn_{1.5}Ni_{0.5}O_4$	$Li_{0.5}Mn_{1.5}Ni_{0.5}O_4$	$Mn_{1.5}Ni_{0.5}O_4$
FM	-526.2873	-498.4072	-470.7362
FiM	**-526.5771**	**-498.6816**	–
AFM1	-526.3859	-498.6534	-470.6744
AFM2	-526.2743	-498.5037	**-470.7813**

Table SI.5: Energy calculated using HSE06 (α=0.25) functional with various initial magnetic structure (eV). Bold values are the minimum value for each composition. FM: ferromagnetic, FiM: ferrimagnetic, AFM1: antiferromagnetic 1, AFM2: antiferromagnetic 2.

Species	**Magnetic moment**			
	PBE	PBE+U	r^{2}SCAN	HSE06
Ni^{2+} ($\mu_{Ni^{2+}}$ = 2S = 2 μ_B)	-1.313	-1.741	-1.561	-1.674
Mn^{4+} ($\mu_{Mn^{4+}}$ = 2S = 3 μ_B)	2.718	3.136	2.848	2.979
M (μ_B)	3.421	3.834	3.492	3.632

Table SI.6: Magnetic moments of Ni^{2+} and Mn^{4+} ions in $LiMn_{1.5}Ni_{0.5}O_4$, calculated using the four functionals evaluated in this work. The resulting magnetisation M is also reported.

Species	**Magnetic moment**				
	$\alpha = 0.25$	$\alpha = 0.19$	$\alpha = 0.18$	$\alpha = 0.17$	$\alpha = 0.15$
Ni^{2+} ($\mu_{Ni^{2+}}$)	-1.674	-1.632	-1.624	-1.615	-1.596
Mn^{4+} ($\mu_{Mn^{4+}}$)	2.979	2.933	2.925	2.916	2.898
M (μ_B)	3.632	3.584	3.576	3.567	3.549

Table SI.7: Magnetic moments of Ni^{2+} and Mn^{4+} ions in $LiMn_{1.5}Ni_{0.5}O_4$, calculated using HSE06 with different mixing parameter α. The resulting magnetisation M is also reported.

4 $Li_{0.5}Mn_{1.5}Ni_{0.5}O_4$ and $Mn_{1.5}Ni_{0.5}O_4$ calculated bond lengths

Distance (Å)	**DFT Results for $Li_{0.5}Mn_{1.5}Ni_{0.5}O_4$**			
	PBE AFM1	PBE+U FM	r^{2}SCAN AFM1	HSE06 FiM
Cell param. a	8.1398	8.2395	8.0600	8.0669
Ni-O (x1)	1.910	1.971	1.890	1.904
Ni-O (x1)	1.990	2.094	1.982	1.890
Ni-O (x1)	2.013	1.965	1.999	2.054
Ni-O (x1)	1.988	1.939	1.972	2.053
Ni-O (x1)	2.004	2.089	2.000	1.903
Ni-O (x1)	1.884	1.956	1.866	1.888
Mn-O (x1)	1.885	1.948	1.875	1.848
Mn-O (x1)	1.941	1.943	1.924	1.904
Mn-O (x1)	1.936	1.947	1.915	1.907
Mn-O (x1)	1.915	1.924	1.899	1.877
Mn-O (x1)	1.909	1.940	1.895	1.902
Mn-O (x1)	1.925	1.918	1.910	1.925

Table SI.8: Cell parameter and M-O bond lengths (M = Ni, Mn) of $Li_{0.5}Mn_{1.5}Ni_{0.5}O_4$ extracted from DFT calculations performed with PBE, PBE+U, r^{2}SCAN and HSE06 ($\alpha = 0.25$) functionals. For comparison, the experimental cell parameter reaches 8.0869(2) Å. The lower symmetry of the $P2_13$ space group leads to various bond lengths.

Distance (Å)	**DFT Results for $Li_{0.5}Mn_{1.5}Ni_{0.5}O_4$**			
	PBE AFM2	PBE+U FM	r^{2}SCAN AFM2	HSE06 AFM2
Cell param. a	8.0679	8.1592	7.9735	7.9721
Ni-O (x1)	1.897	1.902	1.872	1.860
Ni-O (x1)	1.897	1.902	1.872	1.860
Ni-O (x1)	1.898	1.902	1.872	1.860
Ni-O (x1)	1.901	1.902	1.873	1.861
Ni-O (x1)	1.898	1.902	1.872	1.860
Ni-O (x1)	1.901	1.902	1.873	1.861
Mn-O (x1)	1.916	1.936	1.901	1.897
Mn-O (x1)	1.924	1.933	1.902	1.897
Mn-O (x1)	1.916	1.941	1.902	1.895
Mn-O (x1)	1.911	1.933	1.897	1.893
Mn-O (x1)	1.910	1.941	1.900	1.894
Mn-O (x1)	1.905	1.936	1.896	1.891

Table SI.9: Cell parameter and M-O bond lengths (M = Ni, Mn) of $Mn_{1.5}Ni_{0.5}O_4$ extracted from DFT calculations performed with PBE, PBE+U, r^{2}SCAN and HSE06 ($\alpha = 0.25$) functionals. For comparison, the experimental cell parameter reaches 8.0011(2) Å. The antiferromagnetic ordering induces a small symmetry breaking.

5 Varying the α mixing coefficient of HSE06

HSE06 hybrid functional is an exchange-correlation functional composed of an α fraction of Hartree-Fock exchange functional $E_x^{HF,SR}(\mu)$ completed by (1 - α) PBE exchange $E_x^{PBE,SR}(\mu)$ over the short range (SR) and the PBE exchange only over the long range (LR) $E_x^{PBE,LR}(\mu)$ [2, 3]. μ is the screening parameter that determines the separation between SR and LR. The correlation functional is the PBE correlation functional E_c^{PBE}:

$$E_{xc}^{HSE} = \alpha E_x^{HF,SR}(\mu) + (1-\alpha)E_x^{PBE,SR}(\mu) + E_x^{PBE,LR}(\mu) + E_c^{PBE} \quad (1)$$

In VASP, parameter μ is set to 0.2 $Å^{-1}$ and mixing parameter α to 25 % by default.

As pointed out by Chevier *et al.* [4], HSE06 with default mixing parameter tends to overestimate the calculated voltage of lithiated nickel compounds such as the lamellar oxide $LiNiO_2$ or the phosphate $LiNiPO_4$. Adjusting the mixing parameter α was proposed to obtain a better description of the electrochemical properties [5]. By varying α, the average voltage $\overline{V}$ can be tuned to fit the experimental value. Roughly, the average voltage $\overline{V}$ evolves linearly with α [4, 5].

Various calculations were performed with parameter α between 0.15 and the default value of 0.25 (see Table SI.8). The average voltage between $LiMn_{0.5}Ni_{0.5}O_4$ and $Mn_{0.5}Ni_{0.5}O_4$ $\overline{V}$ increases almost linearly with α (see Figure SI.2). $\overline{V}$ reaches 4.996 V for $\alpha = 0.25$ and decreases to 4.560 V for $\alpha = 0.15$. A similar trend was observed by Seo *et al.* [5] for lamellar transition metal oxides. Thus, the optimum mixing parameter to fit the experimental average voltage should be around 0.19.

Composition	Mixing parameter α					**Exp.** [6]	**Exp. (this work)**
	0.15	0.17	0.18	0.19	0.25		
E[$LiMO$] (eV)	-475.409	-485.512	-490.589	-495.673	-526.577		
E[$Li_{0.5}MO$] (eV)	-449.391	-459.106	-463.992	-468.884	-498.682		
E[MO] (eV)	-423.357	-432.715	-437.489	-442.154	-470.781		
E[Li (Metal)] (eV)	-3.894	-3.906	-3.913	-3.919	-3.957		
$\overline{V}$ average (V)	4.560	4.647	4.681	4.730	4.996	4.728	4.731
$\overline{V}$ (Ni^{3+}/Ni^{2+}) (V)	4.557	4.648	4.693	4.738	4.995	4.718	4.724
$\overline{V}$ (Ni^{4+}/Ni^{3+}) (V)	4.561	4.641	4.669	4.723	4.997	4.739	4.739
ΔV (mV)	4	-7	-24	-15	2	21	15

Table SI.10: Energies (in eV) and operating Li/Li^+ voltages (in V) for $Li_xMn_{1.5}Ni_{0.5}O_4$ for (0, 0.5 and 1) calculated using HSE06 by varying the mixing percentage of the exact Hartree-Fock exchange α. The magnetic structures used are then ferrimagnetic for $LiMn_{1.5}Ni_{0.5}O_4$ and $Li_{0.5}Mn_{1.5}Ni_{0.5}O_4$ while $Mn_{1.5}Ni_{0.5}O_4$ is antiferromagnetic. MO stand for $Mn_{1.5}Ni_{0.5}O_4$.

Structural parameters such as the cell parameter and selected bond lengths extracted from calculations performed with various α are displayed in Table SI.11 for $LiMn_{1.5}Ni_{0.5}O_4$. The cell parameter for a mixing parameter of 0.19 is in excellent agreement with the experimental cell parameter measured at 10 K. Ni-O bond lengths are slightly overestimated

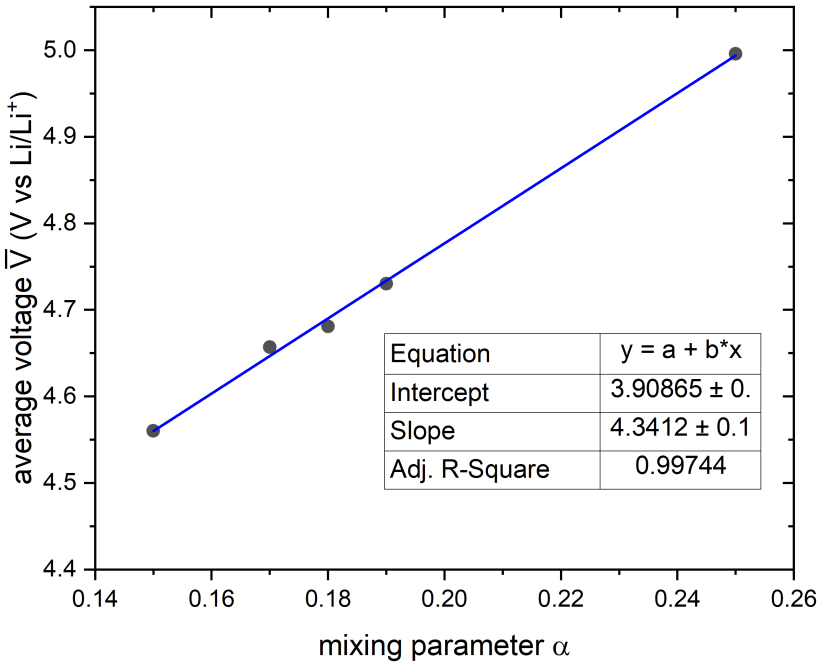

Figure SI.3: Variation of the average voltage $\overline{V}$ with the mixing parameter α of the HSE06 functional.

for all the tested mixing parameter while Mn-O bond lengths tend to be slightly underestimated. However, the overall structural parameters are in good agreement with the experimental data in the mixing parameter range 0.17-0.19.

The difference between the two voltage plateaus ΔV attributed to the two involved redox couples Ni^{3+}/Ni^{2+} and Ni^{4+}/Ni^{3+} with the default mixing parameter α is very small, lower than 2 meV. Decreasing α down to 0.18 turns ΔV to negative values, reaching -24 mV. This peculiar behavior indicates that, depending of the chosen mixing parameter, the stability of the intermediate phase $Li_{0.5}Mn_{0.5}Ni_{0.5}O_4$ is not always observed. However, the amplitude of ΔV in the full range of mixing parameter α remains small, around less than 24 mV.

The energy of $Li_{0.5}Mn_{1.5}Ni_{0.5}O_4$ does not exceed by more than ~ 6 meV/unit formula the energy average of $LiMn_{1.5}Ni_{0.5}O_4$ and $Mn_{1.5}Ni_{0.5}O_4$. Since this difference is limited, a possible explanation is the difficulty to describe accurately the half-lithiated phase $Li_{0.5}Mn_{1.5}Ni_{0.5}O_4$. The 6 Ni-O bonds around Ni^{3+} exhibit a Jahn-Teller distortion, a supercell might be necessary to take into account this effect. Indeed, since there is 4 nickel ions per cell, it is not possible to distort the NiO_6 octahedrons in a manner that conserves the cubic shape of the cell.

Distance (Å)	**Mixing parameter α**					**Exp. (this work)**	
	0.15	0.17	0.18	0.19	0.25	at 10 K	at RT
Cell param. a	8.1706 *+0.14 %*	8.1657 *+0.08 %*	8.1634 *+0.05 %*	8.1608 *+0.02 %*	8.1452 *-0.17 %*	8.1594(1)	8.1692(1)
Ni-O2 (x6)	2.059 *+0.45 %*	2.059 *+0.46 %*	2.060 *+0.50 %*	2.060 *+0.47 %*	2.059 *+0.43 %*	2.050 (1)	2.063 (1)
Mn-O1 (x2)	1.934 *-0.61 %*	1.932 *-0.71 %*	1.931 *-0.76 %*	1.930 *-0.80 %*	1.925 *-1.10 %*	1.946(2)	1.940(2)
Mn-O2 (x2)	1.904 *-0.05 %*	1.902 *-0.14 %*	1.901 *-0.19 %*	1.901 *-0.23 %*	1.89545 *-0.50 %*	1.905(1)	1.907(1)
Mn-O2 (x2)	1.872 *+0.27 %*	1.870 *+0.18 %*	1.870 *+0.14 %*	1.869 *+0.10 %*	1.865 *-0.12 %*	1.867(2)	1.874(1)
Li-O1 (x1)	1.953 *-0.04 %*	1.952 *-0.09 %*	1.951 *-0.10 %*	1.951 *-0.17 %*	1.961 *-0.21 %*	1.957(3)	1.954(3)
Li-O2 (x3)	1.965 *+0.53 %*	1.965 *+0.50 %*	1.964 *+0.48 %*	1.964 *+0.47 %*	1.948 *+0.59 %*	1.954(3)	1.955(3)

Table SI.11: Selected bond lengths extracted from DFT calculations performed with mixing parameter α percentage variation in HSE06 functionals compared with data extracted from PND recorded at 10 K and room temperature (RT). Percentage of variation are calculated relative to the 10 K PND data (italics values). This table represents the variation of the lattice parameter with respect to the experimental lattice parameter for the $LiMn_{1.5}Ni_{0.5}O_4$ structures with (Mn $\uparrow$ Ni $\downarrow$) a ferrimagnetic configuration. The bond lengths of the octahedral and tetrahedral sites of the Mn, Ni and Li cations are shown for the $LiMn_{1.5}Ni_{0.5}O_4$ composition calculated with different types of exchange-correlation functional

6 Bader Charges calculated with the different functionals

Bader charges were computed using the Bader code [7–10]. The average charges of oxygen ions were calculated by considering the crystallographic site multiplicity. The variation values correspond to the difference between the smallest and the highest values of a specific species.

Structures	**Species** (multiplicity)	**Bader Charge**				
		PBE	PBE+U	r^{2}SCAN	HSE06	Variation
$LiMn_{1.5}Ni_{0.5}O_4$	Li (8)	0.893	0.894	0.902	0.900	0.009
	Ni (4)	1.191	1.244	1.285	1.307	0.116
	Mn (12)	1.764	1.860	1.918	1.975	0.211
	O1 (8)	-1.047	-1.057	-1.093	-1.120	0.073
	O2 (24)	-1.029	-1.083	-1.110	-1.132	0.103
	O (average)	-1.038	-1.070	-1.102	-1.126	0.088
$Li_{0.5}Mn_{1.5}Ni_{0.5}O_4$	Li (4)	0.894	0.895	0.902	0.900	0.008
	Ni (4)	1.314	1.346	1.431	1.486	0.172
	Mn (12)	1.794	1.850	1.902	1.962	0.168
	O1 (4)	-0.915	-0.928	-0.962	-0.987	0.072
	O2 (4)	-1.037	-1.053	-1.080	-1.106	0.069
	O3 (12)	-1.005	-1.036	-1.064	-1.092	0.087
	O4 (12)	-0.873	-0.901	-0.935	-0.967	0.094
	O (average)	-0.958	-0.980	-1.010	-1.038	0.080
$Mn_{1.5}Ni_{0.5}O_4$	Ni (4)	1.399	1.368	1.496	1.525	0.157
	Mn (12)	1.798	1.849	1.906	1.967	0.169
	O1 (8)	-0.896	-0.929	-0.965	-0.991	0.095
	O2 (24)	-0.833	-0.843	-0.880	-0.908	0.075
	O (average)	-0.865	-0.886	-0.923	-0.950	0.085

Table SI.12: Bader charges calculated using PBE, PBE+U, r^{2}SCAN and HSE06 functionals for $LiMn_{1.5}Ni_{0.5}O_4$, $Li_{0.5}Mn_{1.5}Ni_{0.5}O_4$, and $Mn_{1.5}Ni_{0.5}O_4$.

References

[1] I. Kishida, K. Orita, A. Nakamura, and Y. Yokogawa, "Thermodynamic analysis using first-principles calculations of phases and structures of $Li_xNi_{0.5}Mn_{1.5}O_4$ ($0 \leq x \leq 1$)," *Journal of power sources*, vol. 241, pp. 1–5, 2013.

[2] A. V. Krukau, O. A. Vydrov, A. F. Izmaylov, and G. E. Scuseria, "Influence of the exchange screening parameter on the performance of screened hybrid functionals," *The Journal of chemical physics*, vol. 125, no. 224106, 2006.

[3] J. Heyd, G. E. Scuseria, and M. Ernzerhof, "Hybrid functionals based on a screened coulomb potential," *The Journal of chemical physics*, vol. 118, no. 18, pp. 8207–8215, 2003.

[4] V. L. Chevrier, S. P. Ong, R. Armiento, M. K. Y. Chan, and G. Ceder, "Hybrid density functional calculations of redox potentials and formation energies of transition metal compounds," *Phys. Rev. B*, vol. 82, p. 075122, Aug 2010.

[5] D.-H. Seo, A. Urban, and G. Ceder, "Calibrating transition-metal energy levels and oxygen bands in first-principles calculations: Accurate prediction of redox potentials and charge transfer in lithium transition-metal oxides," *Phys. Rev. B*, vol. 92, p. 115118, Sep 2015.

[6] K. Ariyoshi, Y. Iwakoshi, N. Nakayama, and T. Ohzuku, "Topotactic two-phase reactions of $Li[Ni_{1/2}Mn_{3/2}]O_4$ ($P4_332$) in nonaqueous lithium cells," *Journal of The Electrochemical Society*, vol. 151, no. 2, p. A296, 2004.

[7] W. Tang, E. Sanville, and G. Henkelman, "A grid-based bader analysis algorithm without lattice bias," *Journal of Physics: Condensed Matter*, vol. 21, no. 8, p. 084204, 2009.

[8] E. Sanville, S. D. Kenny, R. Smith, and G. Henkelman, "Improved grid-based algorithm for bader charge allocation," *Journal of computational chemistry*, vol. 28, no. 5, pp. 899–908, 2007.

[9] G. Henkelman, A. Arnaldsson, and H. Jónsson, "A fast and robust algorithm for bader decomposition of charge density," *Computational Materials Science*, vol. 36, no. 3, pp. 354–360, 2006.

[10] M. Yu and D. R. Trinkle, "Accurate and efficient algorithm for bader charge integration," *The Journal of chemical physics*, vol. 134, no. 6, 2011.